Biophysical Journal, Volume *113*

Supplemental Information

Rapid SNARE-mediated Fusion of Liposomes and Chromaffin Granules with Giant Unilamellar Vesicles

Agata Witkowska and Reinhard Jahn

Supporting Material to

Rapid SNARE-mediated fusion of liposomes and chromaffin granules with giant unilamellar vesicles

Agata Witkowska[1,2] and Reinhard Jahn[1]

[1]Department of Neurobiology, Max-Planck-Institute for Biophysical Chemistry, 37077 Göttingen, Germany

[2]International Max Planck Research School for Molecular Biology at the University of Göttingen, Germany

DOI: http://dx.doi.org/10.1016/j.bpj.2017.03.010

Supporting Figures

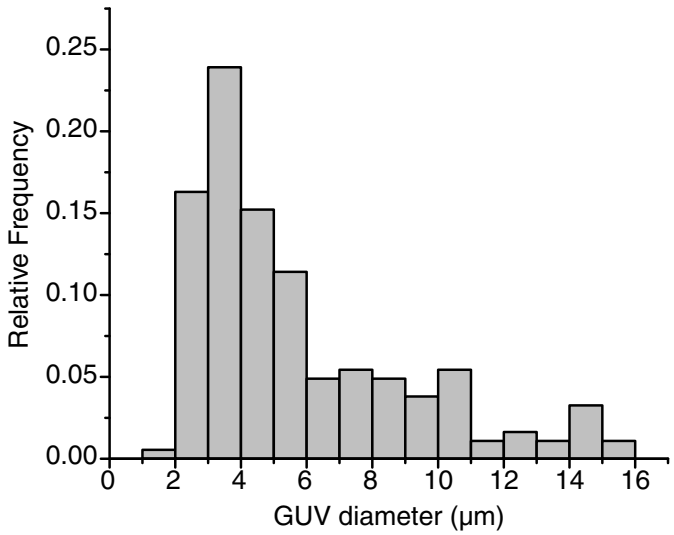

Figure S1. Distribution of diameters of ΔN-GUVs. Histogram presenting relative frequency distribution of diameters of ΔN-GUVs used in this study. It must be noted that GUVs coming from different preparations varied in size distribution, however diameters rarely exceeded 16 µm (n = 184, bin = 1 µm). For experiments involving widefield microscopy (Fig. 2 *b*) larger GUVs were chosen (with diameters >5 µm) that reduced fluorescence coming from GUV membrane localized out-of-focus. On the other hand, for imaging of single vesicles rather smaller GUVs were taken (diameters up to 3 µm) that allowed for reduced acquisition time while keeping relatively small pixel size.

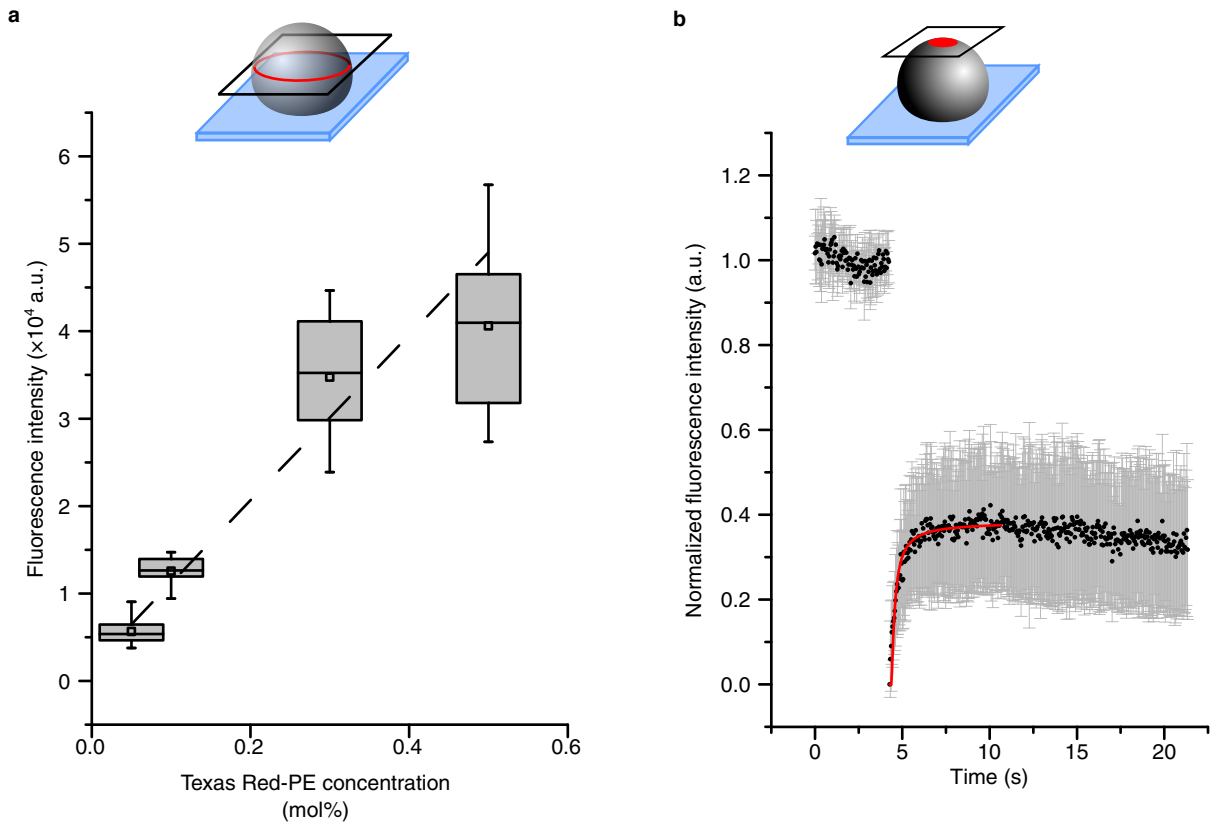

Figure S2. High efficiency of acceptor complex reconstitution into GUVs. (*a*) Calibration curve (dashed line) for the acceptor complex membrane intensity determination created by measuring membrane intensities for various TR-PE concentrations in GUVs (box plots, description as in Fig. 2; $n = 15, 17, 23,$ and 14 starting from 0.05 mol% TR-PE, respectively). (*b*) Representative example of a mean FRAP recovery curve (black dots, grey error bars represent SD, $n = 9$) for TR-PE used for diffusion coefficient determination (Fig. 1 *b*) with a Soumpasis model (fit shown with a red line).

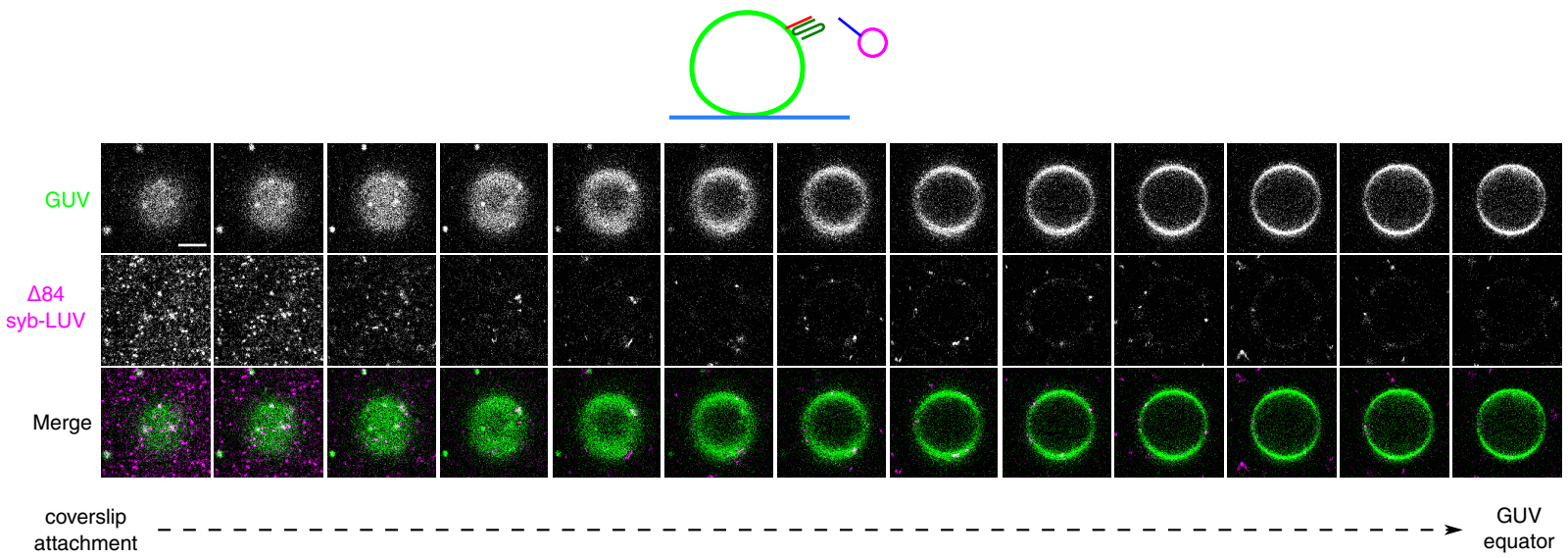

Figure S3. Coverslip related artefacts of liposome attachment. A representative z-stack showing the lower hemisphere of a GUV (labeled with DiO) attached to a coverslip after prolonged incubation (30 min) with Δ84 syb LUVs (DiD). LUVs dock and diffuse on the GUV membrane, some stay in the solution and many become adsorbed at the coverslip surface. Scale bar 5 µm, z-slices are separated by 0.6 µm.

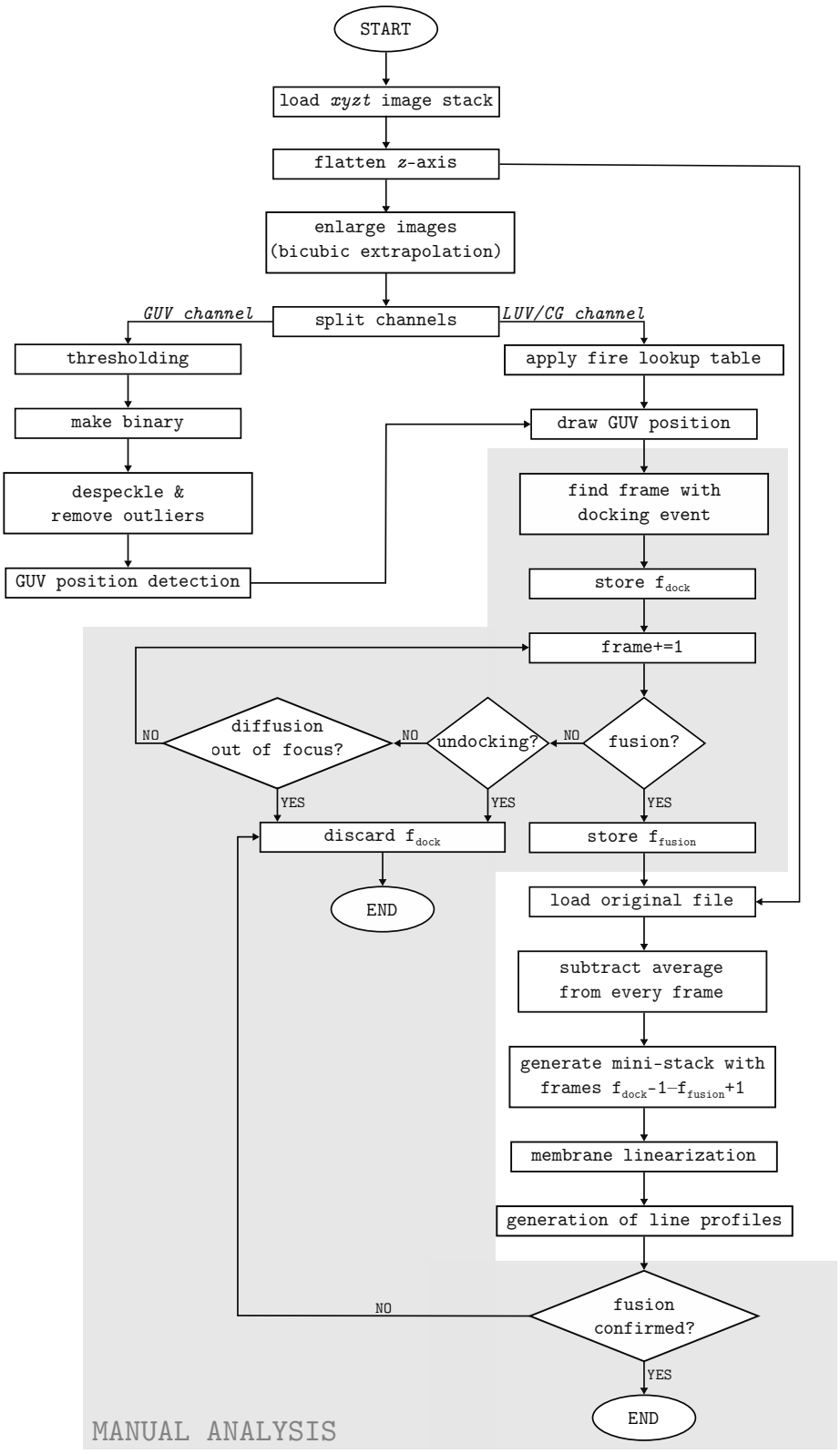

Figure S4. Analysis of single vesicle events. Flowchart representing analysis workflow for detection of a single fusion event, from initial docking to membrane merger. Analysis was automatized except for the part shaded in grey that was done manually. With $\mathtt{f_{dock}}$ and $\mathtt{f_{fusion}}$ labeled the first docking frame and fusion frame, respectively. For description of membrane linearization see Fig. S5 and ref. 6, and for examples of fusion, undocking and diffusion out of focus see Fig. S6.

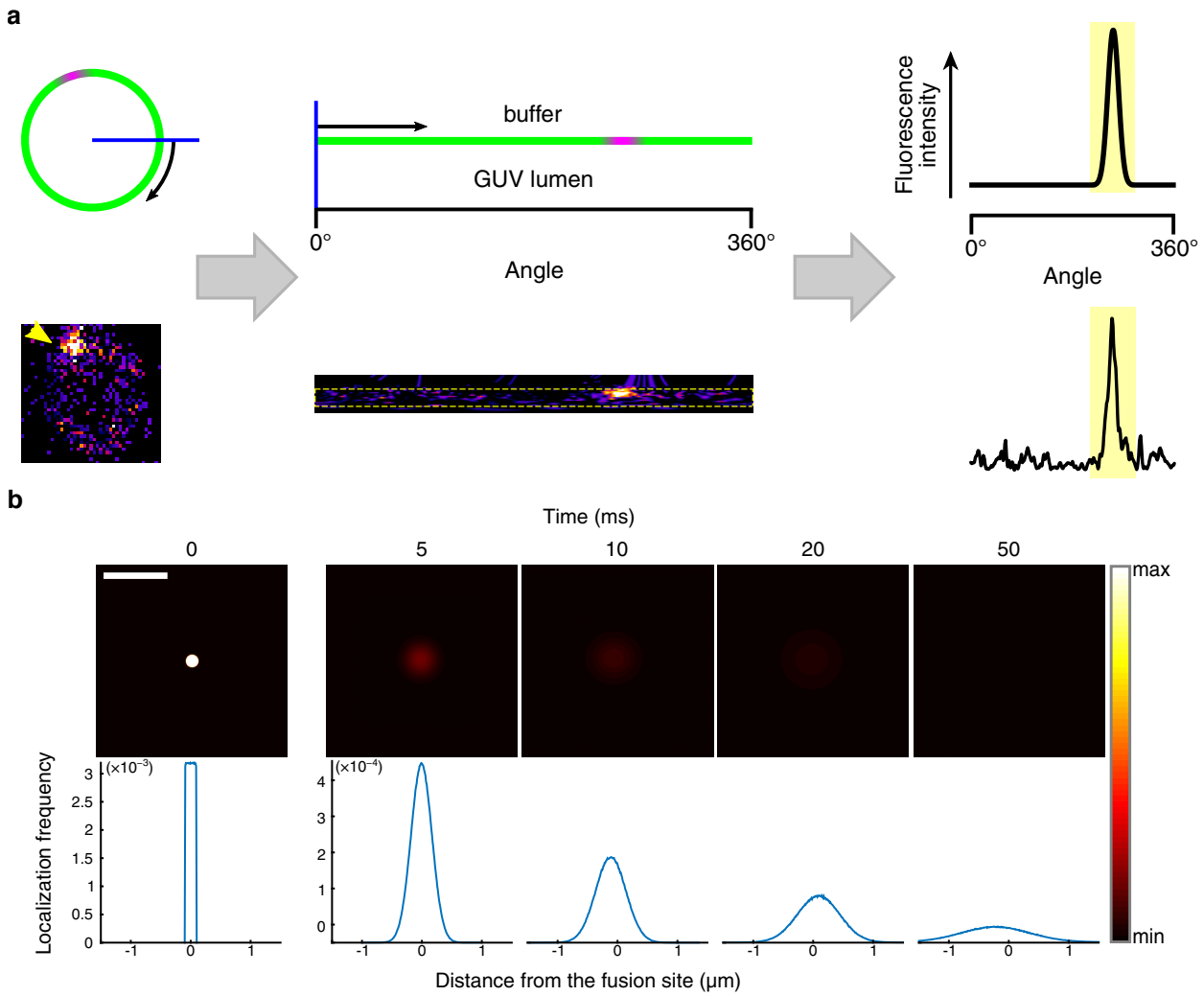

Figure S5. Detection of single vesicle events. (*a*) Schematic illustration of image processing (upper panel) used to aid detection of single vesicle fusion. Corresponding example images and graphs are presented in the lower panel. Images taken for line profiles were normalized by subtracting an averaged stack image from every time frame (resulting image on the left, corresponds to image at $t = 12\,\text{ms}$ in the Fig. 3 *a*). Subsequently, image with centered GUV was transformed to polar coordinates (central panel, see Code availability section) in order to obtain a fluorescence intensity profile (right panel) of membrane-localized region of interest (indicated with a yellow dashed line on the polar-transformed image). Docking events were monitored in the subsequent imaging frames by inspecting line intensity profiles in the region directly corresponding or adjacent to the initial docking spot (i.e. a region max. 45° wide), provided that no undocking nor diffusion out of focus occurred (see Fig. S4 and Fig. S6). An event was categorized as fusion only if in the frame following the docking event the fluorescence signal was present and lower than that of the initial peak. (*b*) Image sequence presenting snapshots of the simulation of post-fusion diffusion of dye molecules in a flat membrane. At the time of fusion ($t = 0\,\text{ms}$), a patch (200 nm in diameter, resulting from incorporation of a membrane coming from a 100 nm LUV) with randomly distributed dye molecules is generated. Subsequently molecules diffuse away from a fusion spot and their density decreases rapidly. Simulation was performed 1×10^5 times (average distribution presented on the snapshots) assuming 985 dye molecules coming from the fusing vesicle, diffusion coefficient of TR-PE (Fig. 1 *b*, $2.83\,\mu\text{m}^2/\text{s}$), and with a time step of 1 ms. Scale bar 1 µm, colormap on the right. Below, shown line profiles passing through the corresponding frame center. Note the different *y*-axis scaling in the frame at $t = 0\,\text{ms}$.

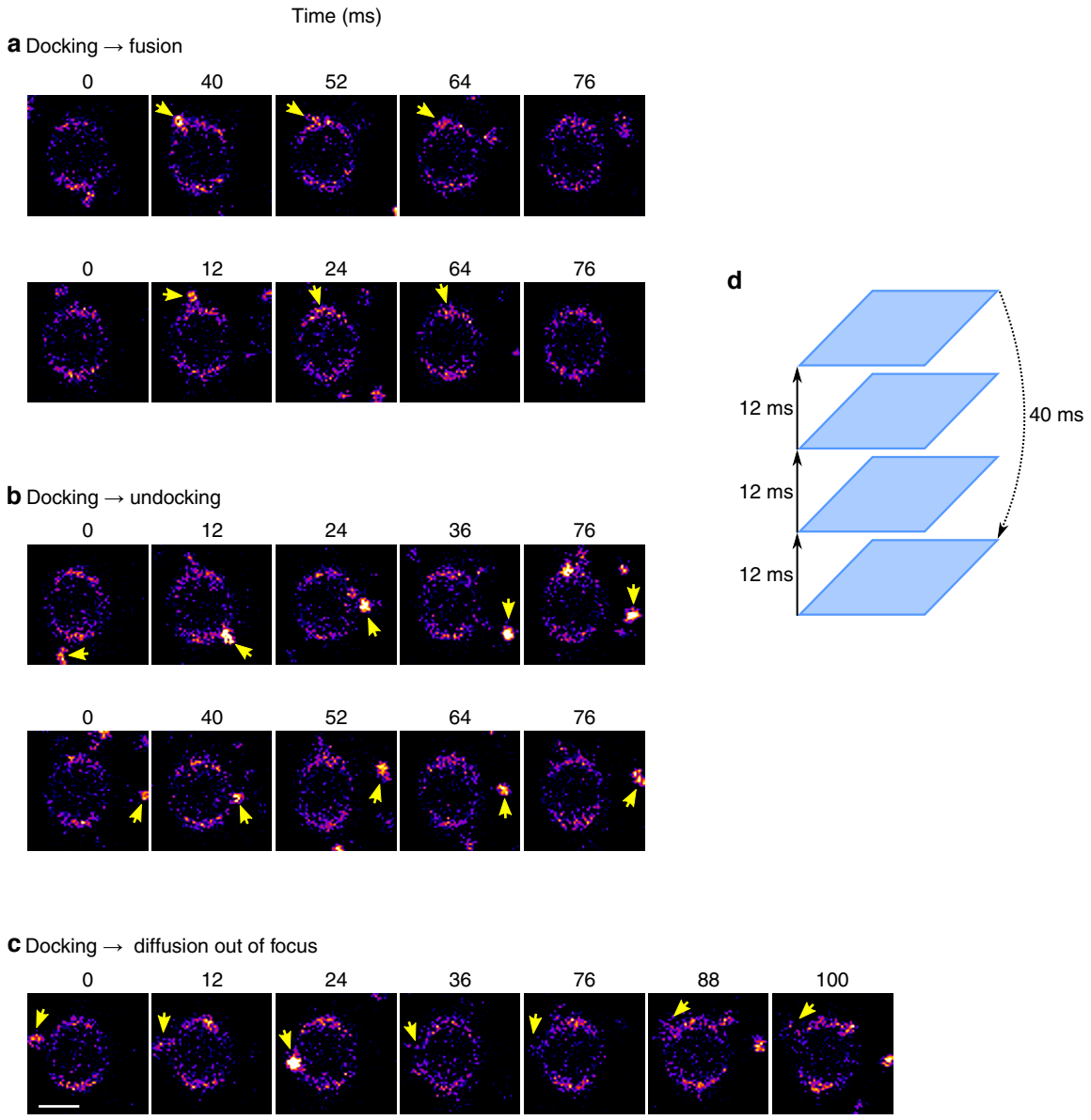

Figure S6. Examples of single vesicle events. Image sequences showing examples of single vesicle events observed in the assay. Presented LUV docking followed by: fusion (*a*), vesicle undocking (*b*), and diffusion on the GUV surface up to a point when it was not visible any more (LUV diffused out of imaged volume, *c*). Scale bar 1 µm. Here undocking (panel *b*) probably arose from random collisions or from the reversible character of a ΔN complex (1–3). It was identified by following the fate of a docked vesicle on subsequent imaging frames. Diffusion of a vesicle out of focus (panel *c*) is characterized by lower fluorescence intensity, enlarged appearance (due to the shape of a point spread function), and lack of visible undocking or fusion. (*d*) Illustration of acquisition workflow and duration of corresponding time frames.

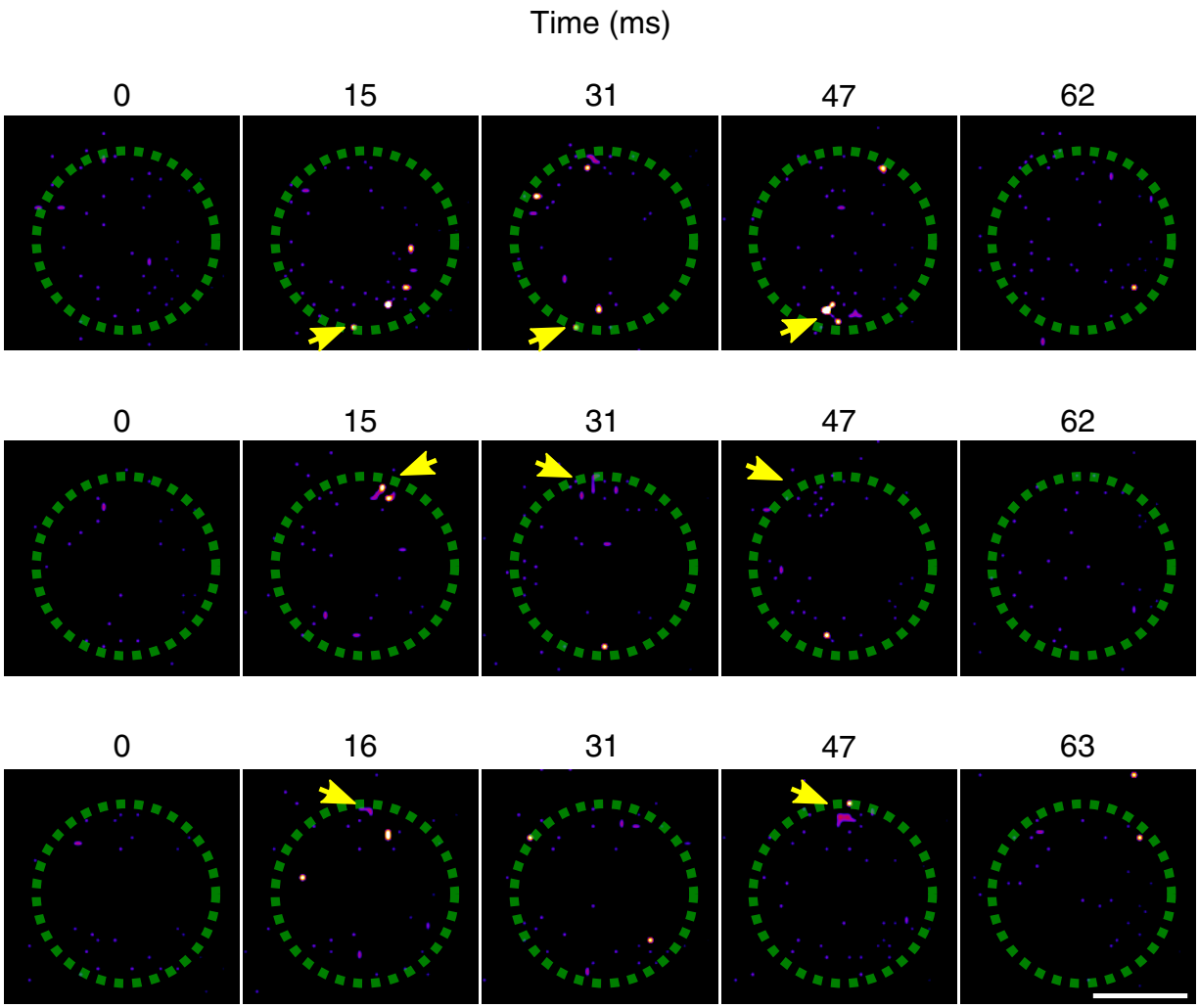

Figure S7. Examples of single vesicle content release events. Image sequences showing examples of bursts of sulforhodamine B fluorescence directed towards the GUV lumen resulting from fusion of syb-SUVs filled with sulforhodamine B at self-quenching concentration (as in Fig. 3 *d*). For clarity, the outline of the GUV (detected in another channel) is indicated by a green dashed line. Scale bar 1 µm.

Supporting Movies

Movie S1. Docking of syb-LUVs onto ΔN-GUV, that is followed by fusion, undocking, or diffusion out of the imaged volume. The same frame size and image processing as in Fig. 3 *b*, movie is slowed down 4×, time stamp located in the corner.

Movie S2. Docking of CGs on ΔN-GUV, that is followed by fusion, undocking, or diffusion out of the imaged volume. The same frame size and image processing as in Fig. 4 *a*, movie is slowed down 4×, time stamp located in the corner.

Supporting Methods

All measurements were done in room temperature.

All histograms and box plots were prepared with Origin (OriginLab, Northampton, MA).

The dye diffusion simulations (Fig. S5) were performed with Octave (4). Source code is available online (5).

Table S1. List of microscope setups used.

Number	Microscope model	Objective	Excitation	Emission	Software	Other
1	Zeiss Axiovert 200M	Plan-Apochromat 100×/1.40 Oil Plan-Apochromat 63×/1.40 Oil DIC	Xenon-short-arc lamp XBO 75	AxioCam MR3	AxioVision	Filter Set 46 (000000-1196-681): BP 500/20, FT 515, BP 535/30 Filter Set 43 (000000-1114-101): BP 545/25, FT 570, BP 605/70 Filter Set 50 (488050-9901-000): BP 640/30, FT 660, BP 690/50
2	Zeiss LSM 780, AxioObserver	LCI Plan-Neofluar 63×/1.3 Imm Korr DIC M27	Lasers: Argon, DPSS561, HeNe594, HeNe633	PMT	Zen 2010	Pinhole 66 µm
3	Leica TCS SP8	HC PL APO CS2 63×/1.40 Oil	Lasers: Argon, DPSS 561, HeNe633	PMT HyD	LAS X	Pinhole 57.2 µm Time interval not always uniform.

Table S2. Specific equipment settings and processing used for listed figures.

Fig.	Microscope (Tab. S1)	Image bit depth	Time and space resolution	Acquisition settings	LUT (linear)	Additional processing and analysis?
Fig. 1*a*, S2*a*	2	16	0.12 µm/px	HeNe594 1% px time = 0.18 ms Emission detection: 600–690 nm, gain 900	—	Membrane linearization macro (6)
Fig. 1b, S2*b*	2	16	0.12 µm/px 40 ms/frame	HeNe594 1%, px time =0.02 ms bleaching 100% laser power, 20 px-wide circular spot, 5 cycles, px time = 0.23 ms Emission detection: 600–690 nm, gain 900	—	FRAP analysis macro (7)
Fig. 2*a*	2	16	0.09 µm/px	NBD: Argon laser 458 nm 2% Emission detection: 496–540 nm, gain 1200 Rho: DPSS 561 0.5% Emission detection: 590–680 nm, gain 900 px time = 22.5 µs bleaching 100% laser power (DPSS 561), circular ROI including whole GUV, 5 cycles, px time = 177.3 µs	NBD: 2000–12000	For quantification, membrane linearization macro (6). Calculated ratio of average NBD membrane fluorescence before and after Rho bleaching (averaged 10 frames before and after bleaching).
Fig. 2*b*	1 100 × objective	12	0.0645 µm/px	Calcein: exposure time = 500 ms, Filter Set 46	Calcein: 200–800	For quantification, membrane linearization macro (6). Measured intensity for ROI representing lumen and membrane of a GUV, subtracted background.

Table S2. continued

Fig.	Microscope (Tab. S1)	Image bit depth	Time and space resolution	Acquisition settings	LUT (linear)	Additional processing and analysis?
Fig. 3*a*	1 63× objective	8	0.102 µm/px	OG: exposure time = 2000 ms, Filter Set 46 TR: exposure time = 500 ms, Filter Set 43	OG: 35–94 TR: 59–10	—
Fig. 3*b*, S5, S6	3	12	0.07 µm/px ∼ 12 ms/frame	8000 Hz, bidirectional scan HeNe 633 0.5% Emission detection: HyD: 650–720 nm nm, gain 150	DiD: 195–1912	See Fig. S4
Fig. 3*d*, S7	3	12	0.061 µm/px ∼ 15.5 ms/frame	8000 Hz, bidirectional scan DPSS 561 2% Emission detection: HyD 570–626 nm , gain 330	SRB: 632–1500	Images displayed: enlarged 4.7× with bicubic extrapolation algorithm
Fig. 4*a*	3	12	0.087 µm/px ∼ 18.5 ms/frame	8000 Hz, bidirectional scan, sequential acquisition of 2 channels TR: DPSS 561 0.3% Emission detection: HyD 570–651 nm, gain 370	TR: 260–3890	See Fig. S4
Fig. S3	2	16	0.1 µm/px $z = 0.3$ µm	DiO: Argon laser 488 nm 1% Emission detection: 496–628 nm, gain 900 DiD: HeNe633 5% Emission detection: 638–755 nm, gain 1020	DiO: 4652–15617 DiD: 3558–26507	Presented every 2nd z-slice

Supporting References

1. Pobbati, A. V., A. Stein, and D. Fasshauer, 2006. N- to C-terminal SNARE complex assembly promotes rapid membrane fusion. Science 313: 673–676.

2. Wiederhold, K., and D. Fasshauer, 2009. Is assembly of the SNARE complex enough to fuel membrane fusion? J. Biol. Chem. 284: 13143–13152.

3. Wiederhold, K., T. H. Kloepper, A. M. Walter, A. Stein, N. Kienle, J. B. Sørensen, and D. Fasshauer, 2010. A Coiled Coil Trigger Site Is Essential for Rapid Binding of Synaptobrevin to the SNARE Acceptor Complex. J. Biol. Chem. 285: 21549–21559.

4. Eaton, J. W., D. Bateman, S. Hauberg, and R. Wehbring, 2016. GNU Octave version 4.2.0 manual: a high-level interactive language for numerical computations.

5. Witkowska, A., 2017. 2D dye diffusion model. doi:10.5281/zenodo.376620.

6. Witkowska, A., 2017. GUV membrane linearization macro. doi:10.5281/zenodo.376618.

7. Witkowska, A., 2017. FRAP analysis macro. doi:10.5281/zenodo.376619.